AGU PUBLICATIONS

Geophysical Research Letters

RESEARCH LETTER
10.1002/2016GL067723

Key Points:
- Significant response in atmospheric frontal frequency to differently resolved Gulf Stream fronts
- Atmospheric response consistent with a thermal air-sea interaction mechanism
- Strong implications for role of frontal air-sea interaction in midlatitude climate variability

Supporting Information:
- Captions for Figures 1–3
- Figure S1
- Figure S2
- Figure S3

Correspondence to:
R. Parfitt,
r.parfitt10@imperial.ac.uk

Citation:
Parfitt, R., A. Czaja, S. Minobe, and A. Kuwano-Yoshida (2016), The atmospheric frontal response to SST perturbations in the Gulf Stream region, *Geophys. Res. Lett.*, *43*, 2299–2306, doi:10.1002/2016GL067723.

Received 13 JAN 2016
Accepted 12 FEB 2016
Accepted article online 15 FEB 2016
Published online 12 MAR 2016

The atmospheric frontal response to SST perturbations in the Gulf Stream region

Rhys Parfitt[1], Arnaud Czaja[1], Shoshiro Minobe[2], and Akira Kuwano-Yoshida[3]

[1]Department of Physics, Imperial College London, London, UK, [2]Department of Natural History Sciences, Graduate School of Science, Hokkaido University, Sapporo, Japan, [3]Application Laboratory, Japan Agency for Marine-Earth Science and Technology, Yokohama, Japan

Abstract The link between sea surface temperature (SST) gradients and atmospheric fronts is explored in a general circulation model across the Gulf Stream (GS) region from December to February 1981–2000. Two model experiments are analyzed, one with a realistic control SST distribution and one with a spatially smoothed SST distribution. The analysis shows a noticeable change in regional atmospheric frontal frequency between the two experiments (up to 30%), with the distribution of change exhibiting a clear imprint of the GS SST front. Further analysis of the surface sensible heat flux gradient across cold fronts reveals the pattern of change to be mediated by a thermal interaction between the oceanic and atmospheric fronts ("thermal damping and strengthening"). These results not only emphasize the significance of the GS SST gradient for storm development in the North Atlantic but also highlight the importance of resolution in assessing the role of frontal air-sea interaction in midlatitude climate variability.

1. Introduction

The ocean carries more heat poleward than the atmosphere at low latitudes, while the reverse occurs at high latitudes. In the Northern Hemisphere, the ocean transfers about 70% of its heat transport to the atmosphere between 25° and 45°N [*Trenberth and Caron*, 2001]. This transfer is mostly in the form of latent and sensible heat fluxes during winter, concentrated over the western boundary currents, the Gulf Stream (GS) in the North Atlantic, and the Kuroshio in the North Pacific. These wintertime fluxes are remarkably variable on a daily timescale and are highly correlated with overlying synoptic atmospheric activity [*Shaman et al*., 2010; *Zolina and Gulev*, 2003]. Locally, these strong oceanic fronts are known to increase the height of the marine atmospheric boundary layer [*Nakamura et al*., 2004], affect cyclogenesis through differential heating [*Persson et al*., 2008; *Giordani and Caniaux*, 2001], and anchor the low-level baroclinicity [*Nakamura et al*., 2008]. Despite this, first-order observations appear to suggest that it is the atmosphere that forces the ocean, and the extent to which extratropical air-sea interactions, in particular ocean-to-atmosphere feedback, affect climate variability is still a contentious issue.

Recently, however, high-resolution studies have shown that the local impact of such oceanic fronts can extend throughout the depth of the troposphere [e.g., *Liu et al*., 2007; *Tokinaga et al*., 2009; *Kobashi et al*., 2008]. In particular, a smoothing of the sea surface temperature (SST) gradient across the GS is shown to alter and reduce the overlying tropospheric vertical motion, both annually and seasonally [*Minobe et al*., 2008; *Kuwano-Yoshida et al*., 2010a], consistent with observational analysis [e.g., *Minobe et al*., 2010]. In wintertime, this mean atmospheric vertical motion over the GS is known to be set by a continuous series of synoptic systems or "baroclinic waveguide" [*Wallace et al*., 1988; *Chang et al*., 2002] that propagate across the region [*Parfitt and Czaja*, 2015]. Together, these studies have interesting implications for understanding the influence of the extratropical oceans on the large-scale atmospheric circulation. They suggest that a key physical process might be the interaction of atmospheric fronts (embedded in the synoptic weather system) with the underlying SST distribution (primarily set by the large-scale ocean circulation). Crucially, this frontal air-sea interaction will most likely depend on the model resolution at which it is considered. As such, as the resolution of general circulation models continues to improve, so too will the mechanism and magnitude of the ocean's role in the general coupled atmosphere-ocean framework, as has been hinted in previous studies. For example, in a recent study by *Smirnov et al*. [2015], an SST anomaly across the Oyashio Extension was shown to produce almost identical vertical profiles of diabatic heating in the overlying atmosphere at coupled resolutions of 1° to 0.25°. However, the increase in resolution from 1° to 0.25° resulted in this heating being balanced by the transient component of the atmospheric circulation, as opposed to a balance by a

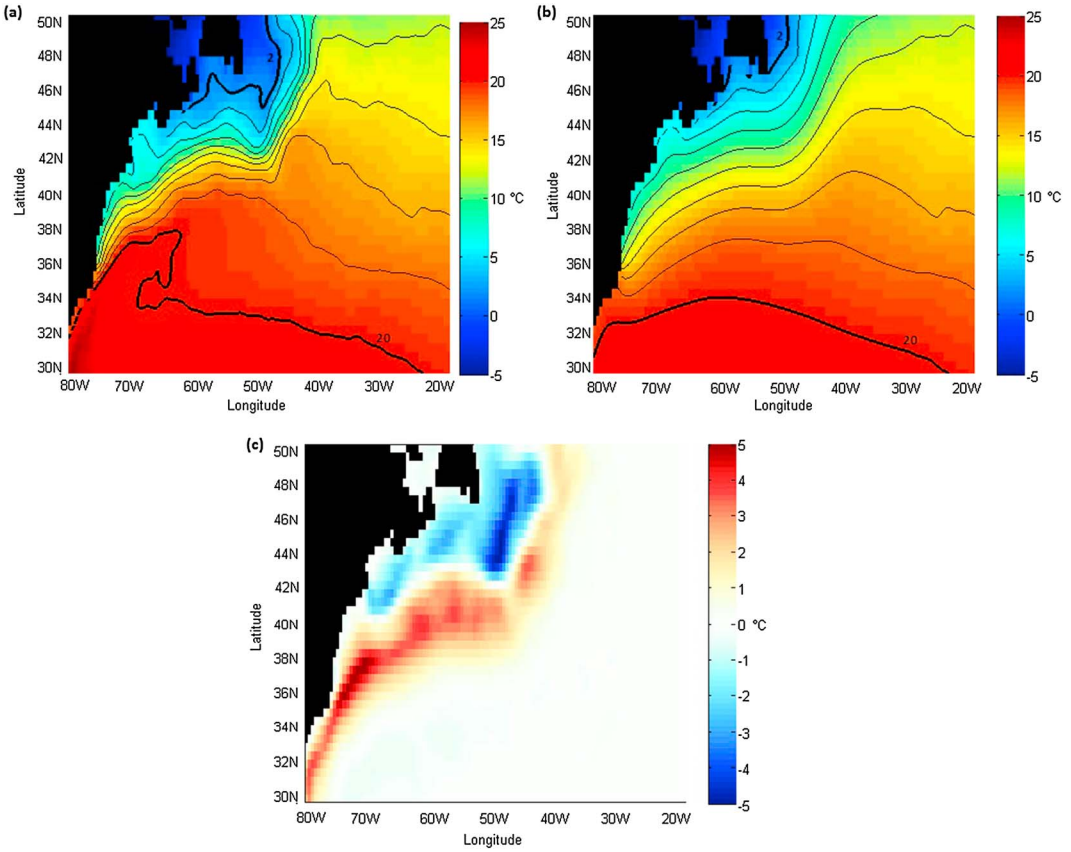

Figure 1. The 20 year wintertime mean (DJF 1981–2000) of SST for the (a) CNTL experiment and (b) SMTH experiment. Black contours are shown from 2°C to 20°C, at 2°C intervals, with the 2°C and 20°C contours thickened. (c) The difference in SST between the CNTL and SMTH experiments.

time-mean flow (as suggested by linear dynamics). In order to better understand the impact of an increased effective resolution for the ocean on the frontal air-sea interaction, the response of atmospheric fronts to a change in SST distribution across the Gulf Stream region is examined.

2. Data and Method

2.1. Model Data Set

The model data to be analyzed are from the atmospheric general circulation model for the Earth Simulator (AFES) version 3 [*Ohfuchi et al.*, 2004; *Enomoto et al.*, 2008; *Kuwano-Yoshida et al.*, 2010b] developed at the Earth Simulator Center, Japan Agency for Marine Earth Science and Technology. The horizontal resolution is T239, about 59 km in grid spacing, with 48 scaled pressure levels in the vertical. The bottom boundary condition in the model uses the NOAA 0.25° daily SST data set [*Reynolds et al.*, 2007]. Data from two experiments are used: a control experiment (CNTL) uses the original real-time global SST data, and the other experiment (SMTH) uses the SST data smoothed over the GS region by applying a 1-2-1 running mean filter in both the zonal and meridional directions 200 times on the 0.25° grid over 25°–50°N, 85°–30°W. Initial conditions are taken from the Japanese 25-year Reanalysis (JRA-25) [*Onogi et al.*, 2007], and the present study uses a 6-hourly output for 20 winter seasons (December-February, DJF), between 1981 and 2000. Figures 1a and 1b show the mean SST for the CNTL and SMTH runs, respectively. The difference in mean SST (CNTL − SMTH), shown in Figure 1c, exhibits a dipolar structure that follows the GS meander. Immediately off the coast, the ocean is colder (warmer) in the CNTL experiment north (south) of ≈40°N than in the SMTH.

2.2. Identification of Atmospheric Fronts

Historically, identification of atmospheric fronts has involved developing a diagnostic quantity based on a chosen variable at a particular atmospheric level. The chosen variable is usually the low-level air temperature (or potential

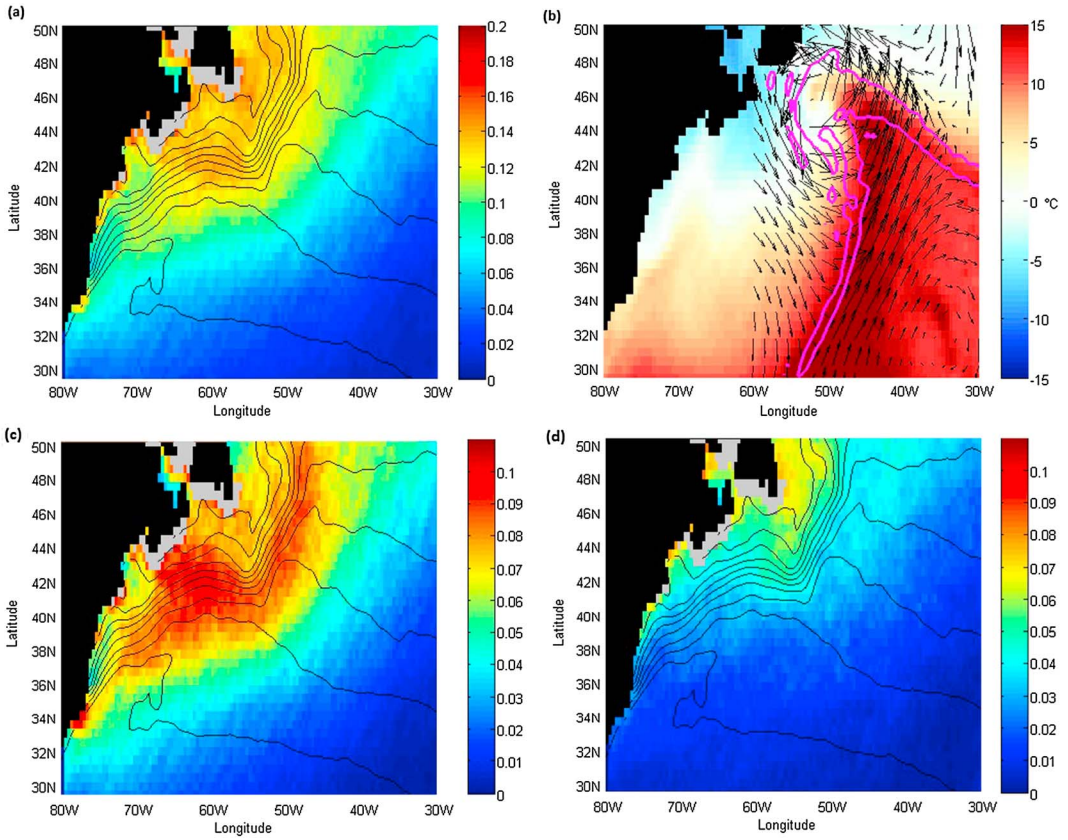

Figure 2. (a) Fraction of wintertime in the CNTL experiment where the front variable *F* exceeds unity. Contours of SST are as in Figure 1a. (b) An atmospheric front, as defined in the text, highlighted in magenta, at 18:00 UTC on 10 December 1983. Also shown at that time are the air temperature at 925 mb (colour) and the horizontal wind direction at 925 mb east of 60°W (black arrows). (c) As in Figure 2a but for cold fronts only. (d) As in Figure 2a but for warm fronts only. Identified coastal regions of overestimation in the frontal frequency (as discussed in the text) are greyed out in Figures 2a, 2c, and 2d. In later figures these regions are simply blacked out with the continent.

temperature), and the method applied is to identify threshold regions of the associated diagnostic, subject to marking criteria where the diagnostic was believed to have been spurious [e.g., *Renard and Clarke*, 1965; *Zwatz-Meise and Mahringer*, 1988; *Steinacker*, 1992; *Hewson*, 1998].

In this paper, the method of identifying fronts follows that introduced in *Sheldon* [2015], in which the frontal diagnostic employs a combination of two atmospheric variables. A measure of front intensity $F^* = \zeta_{925}|\nabla T_{925}|$ is used to identify frontal regions, in which $|\nabla T_{925}|$ is the temperature gradient on the 925 mb surface and ζ_{925} is the component of the curl of the wind vector normal to that same pressure surface (the isobaric relative vorticity). The rationale for this choice is that both $|\nabla T_{925}|$ and ζ_{925} are found to be large in frontal situations [*Sheldon*, 2015]. This is as a result of the transverse circulation developing when cold and warm air masses are brought into contact by a large-scale confluent flow [*Hoskins*, 1982]. In order to make F^* nondimensional (hereafter denoted by *F*), it is further divided by a typical scale for temperature gradient (1 K/100 km) and vorticity (the value of the Coriolis parameter at the midlatitude point of the domain considered, i.e., 40°N). The fronts themselves are identified as locations where $F \geq 1$. This threshold provides a spatial distribution and frequency of frontal events in agreement with other frontal detection methods [e.g., *Berry et al.*, 2011]. The spatial frequency of frontal events (where $F \geq 1$) in the CNTL experiment is illustrated in Figure 2a. Across the GS front, the wintertime frontal frequency ranges from around 10 to 15%. It is noted that the frontal frequency is somewhat overestimated at certain locations along the coastline due to anomalies in the low-level temperature gradient and vorticity that exist at the land-sea boundary. These areas are greyed out in the figure and will not significantly affect the analysis presented in this paper.

In order to further illustrate the detection diagnostic, an atmospheric system is shown in Figure 2b as an example, identified in the CNTL experiment at 18:00 UTC on 10 December 1983. The fronts themselves are highlighted in

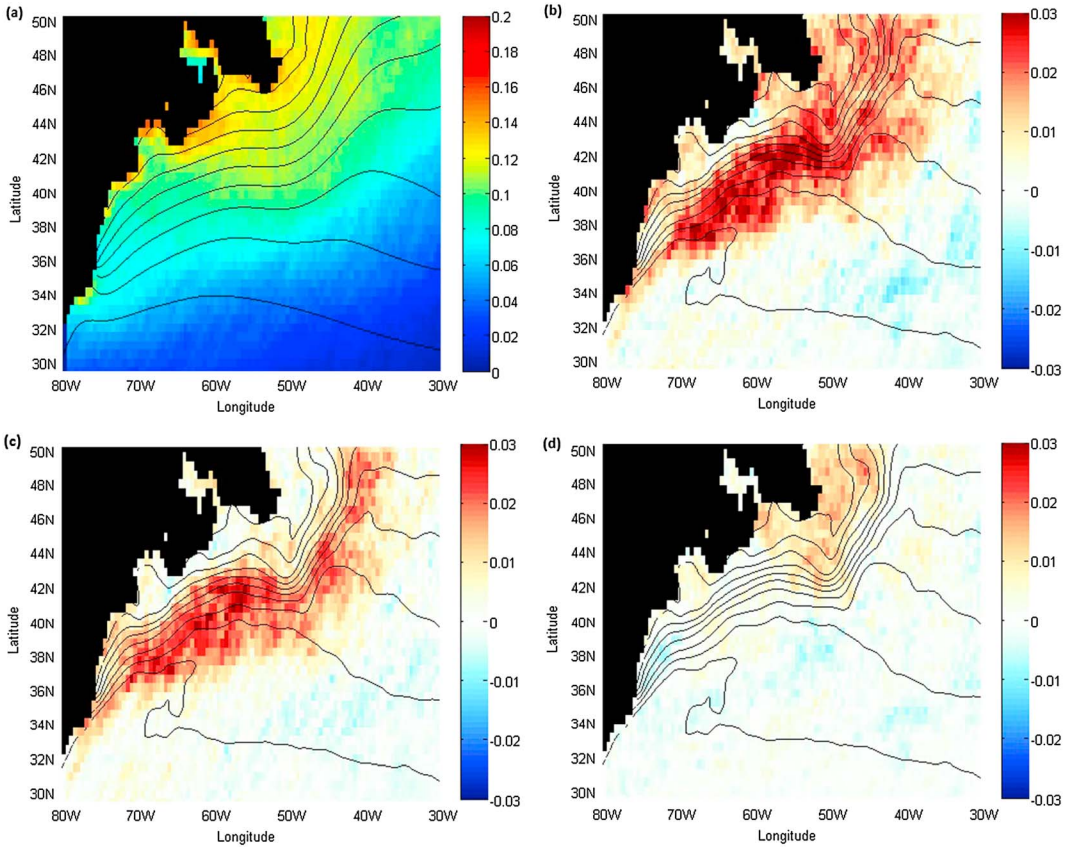

Figure 3. (a) The fraction of wintertime where $F \geq 1$ in the SMTH experiment. Contours of SST are as in Figure 1b. (b–d) The fraction of wintertime where $F \geq 1$ in the CNTL experiment minus the corresponding fraction in the SMTH experiment (i.e., CNTL-SMTH) for (Figure 3b) all fronts, (Figure 3c) cold fronts only, and (Figure 3d) warm fronts only. The mean CNTL SST is shown from 2°C to 20°C, at 2°C intervals (black), for reference. Positive (negative) values imply less (more) frequent fronts in the SMTH experiment than in the CNTL.

magenta (contour $F \geq 1$), while the air temperature at 925 mb is shown in color and the horizontal wind direction east of 60°W on the same pressure level is displayed as arrows. The atmospheric frontal system displays the classic "T" structure associated with a Northern Hemisphere extratropical cyclone. The warm front is located perpendicular to the cold front and wraps around the cyclone centre, about which the winds blow counterclockwise. Behind the primary cold front, there are several secondary cold fronts developing, as is commonly found in observations [e.g., *Browning et al.*, 1997].

In this paper, identified fronts are also separated into cold and warm fronts via calculation of the value of $\boldsymbol{v}_{925}.\nabla T_{925}$, where $\boldsymbol{v}_{925}$ is the horizontal wind vector at 925 mb. In the Northern Hemisphere, the sign of this quantity is expected to be positive (negative) for cold (warm) fronts. The fraction of wintertime in the CNTL experiment where $F \geq 1$ for cold fronts and warm fronts is illustrated in Figures 2c and 2d, respectively. On average in the GS region, cold fronts occur roughly twice as frequently as warm fronts, in agreement with the results of *Berry et al.* [2011].

3. Results

3.1. Atmospheric Frontal Frequency

Figure 3a illustrates the occurrence of $F \geq 1$ in the SMTH experiment. Subsequently, Figure 3b illustrates the difference in the occurrence of $F \geq 1$ between the CNTL experiment with respect to the SMTH experiment (CNTL-SMTH: positive means atmospheric fronts occur more frequently in the CNTL, while negative means less occur in the CNTL), as a fraction of the total wintertime period. It is immediately noticeable that the atmospheric frontal frequency is enhanced in the CNTL experiment across the vast majority of the GS front

(i.e., a strong reduction in the SMTH experiment). This enhancement implies that in the CNTL experiment, atmospheric fronts are identified on around 3% more of the total wintertime period than in the SMTH. While this number may sound rather small, comparison with Figure 3a shows that this corresponds to an atmospheric frontal frequency percentage increase of roughly 30% with regard to the SMTH experiment. This increase is strongly limited to the GS meander and sharply diminishes to zero as one moves away to the south and east. This pattern was consistently found when the same analysis was performed again on randomly sampled periods of 5 years within the same 20 year range, indicating the robustness of the result (not shown).

Figures 3c and 3d illustrate the aforementioned difference between the occurrence of $F \geq 1$ in the CNTL experiment with respect to the SMTH experiment but separately for cold fronts and warm fronts, respectively. Along the entirety of the GS front for regions where the CNTL SST is higher than ≈6°C, there is a fractional increase in wintertime atmospheric cold frontal frequency of around 0.02–0.03 that once again falls sharply to zero as one moves away from the sharp SST gradient (comparable signals can also be found farther from the surface, e.g., 775 mb; see Supporting Information Figure S1). Comparison with Figure 2c shows that as in Figure 3b the relative change is roughly 30%. However, this is not the case for warm fronts, with little change exhibited along most of the GS front. For warm fronts, the majority of the response can be found off the coast north of ≈44°N and west of ≈45°W. Here the fractional increase in warm frontal frequency is around 0.01–0.015, with a relative change of roughly 30% as in the cold frontal case. Nevertheless, it is clear that the overwhelming contributor to the total frontal response seen in Figure 3b can be attributed to the cold frontal response alone. It is noted that this change in cold frontal frequency is affected noticeably by both $|\nabla T_{925}|$ and ζ_{925} (see Supporting Information Figure S2), although the absolute contribution of $|\nabla T_{925}|$ is larger. As shown in the Supporting Information Figure S3, the vertical motion at the fronts is also strengthened in the CNTL experiment compared to the SMTH experiment.

3.2. Thermal Damping and Strengthening of Atmospheric Fronts

It has been shown in section 3.1 that the atmospheric frontal response across the GS front is mostly attributed to the cold fronts. In this section we propose a simple mechanism to explain why this may be so, solely considering the thermal interaction between the ocean and the atmosphere. We refer to this mechanism as "thermal damping and strengthening" (TDS) and illustrate it in Figure 4.

Initially, we consider a highly idealized situation in which a cold front passes over an oceanic front that is aligned such that the ocean temperature is equal to the atmospheric temperature at the surface. In this thermally adjusted or neutral situation, there is no sensible heat exchange between the surface and the atmosphere. A schematic of this is shown in Figure 4a.

Figure 4b shows the case where there is a strong SST gradient (such as the Gulf Stream) aligned in the same direction as the preexisting atmospheric cold front. As a result of this strong SST gradient, there is now a warmer ocean below a warm atmosphere and a colder ocean below a cold atmosphere (the larger temperature anomalies in the ocean are indicated in Figure 4 by bigger letters W and C). This state of affairs leads to a sensible heat exchange between the ocean and the atmosphere which acts toward *strengthening* the atmospheric temperature gradient (and hence the strength of the cold front itself).

Lastly, Figure 4c indicates the case where there is a SST gradient aligned in the opposite direction to the atmospheric frontal temperature gradient. In this case, the induced cross-frontal sensible heat flux exchange will act toward *dampening* the strength of the cold front (in comparison to the situation in Figure 4a).

As is clear from Figure 4, the TDS of atmospheric fronts is modulated by the cross-frontal surface sensible heat flux gradient dQ/dy, where Q is the surface sensible heat flux and y is the cross-frontal directional vector with positive defined as toward the cold sector—this argument is also supported by the classic study by *Eliassen* [1962], who showed that the strength of the transverse circulation at a front can be modulated diabatically by dQ/dy. In turn, dQ/dy depends both on the magnitude of the SST gradient and the relative orientation of the atmospheric and oceanic fronts.

Figure 5a illustrates the 20 year wintertime average of dQ/dy in the CNTL experiment for cold fronts. Whenever a cold front is identified at a certain location in the CNTL experiment, the cross-frontal surface sensible heat flux gradient is calculated as the scalar product between the gradient of the surface sensible heat flux and the unit vector in the direction of the 925 mb temperature gradient. Then, the 20 year average

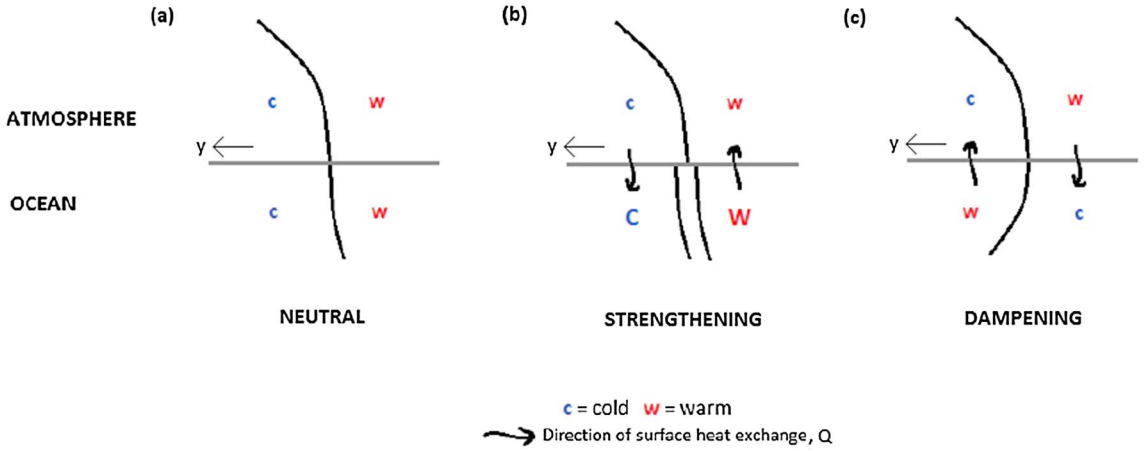

Figure 4. Schematic of an atmospheric cold front passing over (a) an SST gradient aligned such that the ocean temperature is equal to the atmospheric temperature at the surface, (b) a strong SST gradient aligned in the same direction, and (c) an SST gradient aligned in the opposite direction. Black wavy arrows indicate the direction of surface sensible heat fluxes, while the cross-frontal direction vector (*y*) is shown as a thin black arrow (positive toward the cold sector).

at each location is plotted. One can see that along the GS front between roughly 6°C and 14°C, $dQ/dy < 0$, meaning that on average the cross-frontal surface sensible heat flux gradient is acting to enhance the cold fronts in this region. Either side of these SST contours along the front, however, $dQ/dy > 0$, indicates that on average the cross-frontal surface sensible heat flux gradient is acting to dampen the cold fronts here. Naturally, such a tripole pattern along the strong oceanic frontal zone lends itself to atmospheric cold fronts

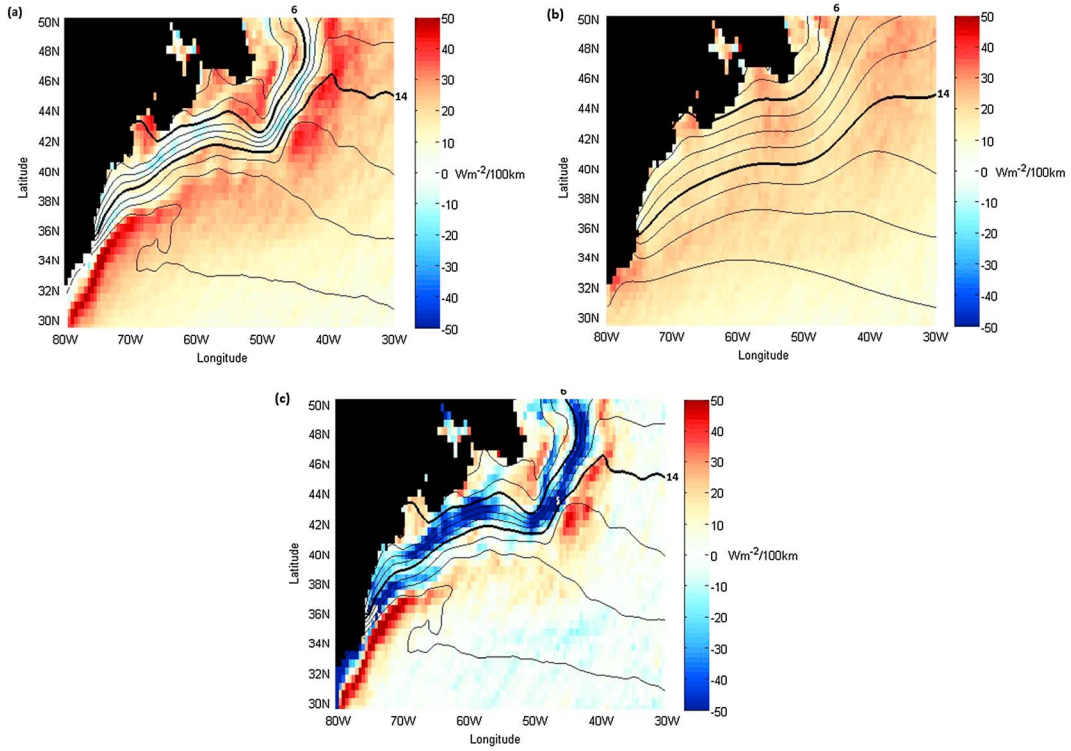

Figure 5. (a) The 20 year wintertime average of the cross-cold-frontal surface sensible heat flux gradient, dQ/dy, (expressed in W m^{-2}/100 km), at each location in the CNTL experiment. Contours of SST are as in Figure 1a, with the 6°C and 14°C contours thickened. (b) As in Figure 5a but for the SMTH experiment. Contours of SST are as in Figure 1b. Positive (negative) values imply that on average dQ/dy acts to thermally dampen (strengthen) passing atmospheric cold fronts at that location. (c) The difference in dQ/dy between the CNTL and SMTH experiments (CNTL-SMTH). Positive (negative) values imply that the cross-frontal surface sensible heat flux gradient acts on average to thermally dampen a cold front more (less) in the CNTL experiment than in the SMTH. Contours of SST are as in Figure 5a.

preferentially intensifying along the GS front. Figure 5b illustrates the 20 year wintertime average of dQ/dy in the SMTH experiment. Unlike the CNTL experiment, there is no analogous region of cold frontal enhancement, with the entire GS region acting to dampen cold fronts that propagate across it. However, the magnitude of this damping is roughly even across the entire region, and the maximum magnitude of damping in regions of the CNTL experiment can reach approximately twice this value. This suggests that despite there being no regions of cold frontal enhancement in the SMTH experiment, there may be regions where the cold fronts are on average damped less than in the CNTL experiment.

Figure 5c illustrates the difference in the average dQ/dy between the CNTL and the SMTH experiments (i.e., CNTL-SMTH, ΔdQ/dy). Regions where $\Delta \mathrm{d}Q/\mathrm{d}y > 0$ (<0) indicate more (less) damping in the CNTL than in the SMTH, and subsequently, one should expect this to result in a lower (higher) frontal frequency in the CNTL than in the SMTH. Comparison with Figure 3c indeed shows this to be the case, albeit with slightly broader regions of change in the frontal frequency. This is due to the advection for the thermal interaction. Given that a typical timescale for air-sea interactions and frontogenesis is ≈1 day and assuming that the associated storm travels at ≈10 m s^{-1}, one can expect a displacement in the cold frontal response to the perturbed surface heat flux gradient of ≈10° longitude, which is what is observed.

4. Conclusions and Discussion

In this paper, the response of atmospheric fronts to a change in the SST gradient in the GS region has been examined in the AFES version 3. It has been shown that a reduction in the SST gradient can result in significant changes to the frequency of atmospheric fronts (a reduction of up to ≈30% across the vast majority of the GS front). These changes are mostly due to the response of the cold fronts. Further results strongly suggest that the mechanism governing the response of these cold fronts to the SST perturbation is thermal damping and strengthening (TDS), related to the magnitude of the cross-frontal surface air-sea heat exchange. Such anomalous cross-frontal heat flux gradients can be caused by a strengthening or weakening of the SST gradient or by changes in the relative orientation of atmospheric fronts with the underlying oceanic fronts, as explained in section 3.2. Specifically, the weaker SST gradient in the SMTH experiment acts solely to thermally damp cold fronts passing above, whereas the stronger SST front present in the CNTL experiment also allows for thermal enhancement of their strength. Changes in circulation (low-level vorticity and upward motion) were found at the fronts, and it is speculated that these might be instrumental in setting the time-mean value of these fields in the Gulf Stream region [*Minobe et al*., 2008; *Parfitt and Czaja*, 2015].

It is noted that the significance of the TDS mechanism proposed in this paper will likely increase its importance as the effective resolution of the atmospheric and oceanic fronts in models and data increases. In fact, the comparison between the SST gradients in the CNTL and SMTH experiments in this paper can reasonably be considered as a comparison between two differently resolved GS fronts at the exact same atmospheric resolution. The clear increase in atmospheric frontal frequency detected with a stronger (or "more resolved") SST gradient strongly suggests that the forcing role of oceanic fronts on atmospheric cold fronts will become more active as the air-sea interactions become better resolved. Determining the magnitude and extent to which an increase in resolution will affect ocean forcing or feedback on the atmosphere, either in a fully coupled model framework or in real-world data itself, is the next important step, especially as the resolution of current coupled climate models continues to increase.

Acknowledgments
This work is part of R.P.'s PhD at Imperial College funded by the UK Natural Environment Research Council. S.M. is supported by the JSPS KAKENHI 26287110 and 15H01606. The data used in this study will be curated for 5 years and are available upon request by contacting the corresponding author.

References

Berry, G., M. J. Reeder, and C. Jakob (2011), A global climatology of atmospheric fronts, *Geophys. Res. Lett.*, *38*, L04809, doi:10.1029/2010GL046451.
Browning, K. A., N. M. Roberts, and A. J. Illingworth (1997), Mesoscale analysis of the activation of a cold front during cyclogenesis, *Q. J. R. Meteorol. Soc.*, *123*(544), 2349–2374.
Chang, E. K., S. Lee, and K. L. Swanson (2002), Storm track dynamics, *J. Clim.*, *15*(16), 2163–2183.
Eliassen, A. (1962), On the vertical circulation in frontal zones, *Geofys. Publ.*, *24*(4), 147–160.
Enomoto, T., A. Kuwano-Yoshida, N. Komori, and W. Ohfuchi (2008), Description of AFES 2: Improvements for high-resolution and coupled simulations, in *High Resolution Numerical Modelling of the Atmosphere and Ocean*, pp. 77–97, Springer, New York.
Giordani, H. and G. Caniaux (2001), Sensitivity of cyclogenesis to sea surface temperature in the northwestern Atlantic, *Mon. Weather Rev.*, *129*(6), 1273–1295.
Hewson, T. D. (1998), Objective fronts, *Meteorol. Appl.*, *5*, 37–65.
Hoskins, B. J. (1982), The mathematical theory of frontogenesis, *Annu. Rev. Fluid Mech.*, *14*(1), 131–151.
Kobashi, F., S. P. Xie, N. Iwasaka, and T. T. Sakamoto (2008), Deep atmospheric response to the North Pacific oceanic subtropical front in spring, *J. Clim.*, *21*(22), 5960–5975.
Kuwano-Yoshida, A., S. Minobe, and S.-P. Xie (2010a), Precipitation response to the Gulf Stream in an atmospheric GCM, *J. Clim.*, *23*(13), 3676–3698.

Kuwano-Yoshida, A., T. Enomoto, and W. Ohfuchi (2010b), An improved PDF cloud scheme for climate simulations, *Q. J. R. Meteorol. Soc.*, *136*, 1583–1597.
Liu, W. T., X. Xie, and P. P. Niiler (2007), Ocean–atmosphere interaction over Agulhas extension meanders, *J. Clim.*, *20*(23), 5784–5797.
Minobe, S., A. Kuwano-Yoshida, N. Komori, S. P. Xie, and R. J. Small (2008), Influence of the Gulf Stream on the troposphere, *Nature*, *452*(7184), 206–209.
Minobe, S., M. Miyashita, A. Kuwano-Yoshida, H. Tokinaga, and S. P. Xie (2010), Atmospheric response to the Gulf Stream: Seasonal variations*, *J. Clim.*, *23*(13), 3699–3719.
Nakamura, H., T. Sampe, Y. Tanimoto, and A. Shimpo (2004), Observed associations among storm tracks, jet streams and midlatitude oceanic fronts, *Geophys. Monogr. Ser.*, *147*, 329–345.
Nakamura, H., T. Sampe, A. Goto, W. Ohfuchi, and S. P. Xie (2008), On the importance of midlatitude oceanic frontal zones for the mean state and dominant variability in the tropospheric circulation, *Geophys. Res. Lett.*, *35*, L15709, doi:10.1029/2008GL034010.
Ohfuchi, W., et al. (2004), 10-km mesh meso-scale resolving simulations of the global atmosphere on the Earth Simulator: Preliminary outcomes of AFES (AGCM for the Earth Simulator), *J. Earth Simul.*, *1*, 8–34.
Onogi, K., et al. (2007), The JRA-25 reanalysis, *J. Meteorol. Soc. Jpn.*, *85*(3), 369–432.
Parfitt, R. and A. Czaja (2015), On the contribution of synoptic transients to the mean atmospheric state in the Gulf Stream region, *Q. J. R. Meteorol. Soc.*, doi:10.1002/qj.2689, in press.
Persson, P. O. G., J. E. Hare, L. B. Nance, and B. Walter (2008), Impact of air-sea interaction on extra-tropical cyclones, in *Proceedings ECMWF Workshop on Ocean-Atmosphere Interactions*, pp. 123–146, ECMWF, Reading, U. K.
Renard, R. J. and L. C. Clarke (1965), Experiments in numerical objective frontal analysis, *Mon. Weather Rev.*, *93*, 547–556.
Reynolds, R. W., T. M. Smith, C. Liu, D. B. Chelton, K. S. Casey, and M. G. Schlax (2007), Daily high-resolution-blended analyses for sea surface temperature, *J. Clim.*, *20*(22), 5473–5496.
Shaman, J., R. M. Samelson, and E. Skyllingstad (2010), Air–Sea fluxes over the Gulf Stream region: Atmospheric controls and trends, *J. Clim.*, *23*(10), 2651–2670.
Sheldon, L. (2015), The role of the deep moist convective processes in western boundary currents-troposphere coupling, 229 pp., PhD thesis, Imperial College, London.
Smirnov, D., M. Newman, M. A. Alexander, Y.-O. Kwon, and C. Frankignoul (2015), Investigating the local atmospheric response to a realistic shift in the Oyashio sea surface temperature front, *J. Clim.*, *28*, 1126–1147.
Steinacker, R. A. (1992), Dynamic aspects of frontal analysis, *Meteorol. Atmos. Phys.*, *48*, 93–103.
Tokinaga, H., S. P. Xie, F. Kobashi, and Y. Tanimoto (2009), Local and remote influences of the Kuroshio Extension on the atmosphere, *US CLIVAR Var.*, *7*, 1–4.
Trenberth, K. E. and J. M. Caron (2001), Estimates of meridional atmosphere and ocean heat transports, *J. Clim.*, *14*(16), 3433–3443.
Wallace, J. M., G. H. Lim, and M. L. Blackmon (1988), Relationship between cyclone tracks, anticyclone tracks and baroclinic waveguides, *J. Atmos. Sci.*, *45*(3), 439–462.
Zolina, O. and S. K. Gulev (2003), Synoptic variability of ocean–atmosphere turbulent fluxes associated with atmospheric cyclones, *J. Clim.*, *16*(16), 2717–2734.
Zwatz-Meise, V. and G. Mahringer (1988), Use of satellite imagery, combined with numerical model diagnostics, to locate fronts and predict their activity: Methods and examples, in *Satellite and Radar Imagery Interpretation, Preprints for a Workshop in Reading, England, 20–24 July 1987*, edited by M. Bader and T. Wcpraters, pp. 143–162, Eumetsat.